Title
POINT DEFECTS AND SINTERING LEAD SIRCONATE TITANATE

Authors
Atkin, R.B.
Fulrath, R.M.

Publication Date
1970-12-01

Submitted to Journal of the American Ceramic Society

UCRL-20309 Rev.
Preprint

c.2

POINT DEFECTS AND SINTERING LEAD ZIRCONATE TITANATE

R. B. Atkin and R. M. Fulrath

December 1970

AEC Contract No. W-7405-eng-48

LAWRENCE RADIATION LABORATORY
UNIVERSITY of CALIFORNIA BERKELEY

UCRL-20309 Rev.

DISCLAIMER

POINT DEFECTS AND SINTERING LEAD ZIRCONATE TITANATE

R. B. Atkin* and R. M. Fulrath

Inorganic Materials Research Division, Lawrence Radiation Laboratory,
and Department of Materials Science and Engineering,
College of Engineering, University of California,
Berkeley, California

ABSTRACT

The crystal chemistry of point defects in lead zirconate titanate is discussed. The results are used to interpret sintering and grain growth behavior.

Lattice vacancies are created thermally, by substitutional impurities with the incorrect valence, and by changing the stoichiometry. Charged oxygen vacancies are introduced when Al^{+3} replaces Ti^{+4} and charged lead vacancies are introduced when Nb^{+5} replaces Ti^{+4}. These vacancies are believed associated with the impurity ions and cause them to be adsorbed at grain boundaries. This retards grain growth and thereby expedites densification. Aluminum ions (deficient valence) compensate for niobium ions (excess valence). These "paired" defects are not associated with vacancies and are not adsorbed so they do not impede grain growth.

Based in part on a thesis submitted by Robert B. Atkin for the D. of Eng. degree in materials science at the University of California, Berkeley, September 1970.

At the time this work was done the writers were, respectively, research assistant and professor of ceramic engineering, Department of Materials Science and Engineering, College of Engineering, and Inorganic Materials Research Division, Lawrence Radiation Laboratory, University of Calif.

*Now with IBM Corp., San Jose, California.

Sintering follows Coble's model, bulk diffusion of vacancies from pores to grain boundaries. Oxygen vacancies are believed to be the slowest moving species. Aluminum:niobium compensation is again observed.

Doping with aluminum decreases the mobility of ferroelectric domain boundaries while niobium increases it. Doping with both ions produce ferroelectric properties similar to undoped material.

I. Introduction

Lead zirconate titanate ceramics are extensively used for piezoelectric devices and are promising candidates for electro-optic and information storage devices. These applications require very precisely controlled ferroelectric properties, hence, close control over the ceramic microstructure and composition is required. To achieve this control, the factors affecting the materials behavior during the fabrication process should be thoroughly understood.

The sintering and grain growth behavior of lead zirconate titanate powder is quite sensitive to additions of certain three and five valent ions.[1] Niobium, for example, accelerates densification.[2] It has been suggested that doping increases the concentration of lattice vacancies, thereby increasing the rate of diffusion and densification; this explanation will be examined. Aluminum ions also affect the behavior of this material.[3-5] This is of considerable practical importance because ceramic processing may introduce relatively large and uncontrolled amounts of aluminum oxide.[6] Powder mixing and grinding operations are often done in porcelain or alumina ball mills with alumina media; normal mill wear will introduce appreciable quantities of alumina, silica and magnesia.[4]

The sintering atmosphere also affects the ultimate microstructure and ferroelectric properties.[4,7] Sintering an oxide compound in a reducing atmosphere will change the concentration of lattice vacancies and, hence, the diffusivities of the oxygen and metal ions. This concept, as applied to the sintering of alumina, has been discussed in detail by Coble.[8]

This paper discusses the chemistry of point defects in lead zirconate titanate and the mechanisms by which these defects determine the sintering and grain growth behavior.

II. Experimental

Batches of lead zirconate titanate and lead zirconate titanate doped with 2 at% niobium were compounded from the appropriate oxides.* After intimate mixing, the materials were calcined in a covered platinum crucible at 850°C. The reacted material was crushed with a lucite mortar and pestle, then ground in a vibratory ball mill with lucite grinding media. This reduced the average crystal size to about one micron and the lucite contaminate was removed by air oxidation at 400°C. Spectrographic analysis showed the materials contained approximately 0.05 wt% Al_2O_3, 0.02 wt% CaO, 0.02 wt% SiO_2 and 0.002 wt% MgO. Additional aluminum (0.4 wt%) was added to a portion of each batch as an aqueous nitrate solution.

Specimens were formed by pressing the powders into pellets in a steel die. These pellets were pre-fired at 800°C for 1 h. This increased their strength sufficiently to allow measurements of their initial dimensions and weight. No significant shrinkage occurred during pre-firing. The weighed and measured pellets were loosely covered with packing powder† in a platinum crucible with a tight fitting lid. The crucible was evacuated and refilled with the desired gas. Oxygen and

---

*Baker reagent grade PbO, Wah Chang reactor grade ZrO_2, B&A reagent grade TiO_2 and Matheson, Coleman & Bell Nb_2O_5.

†The powder is to isolate the specimens and to provide the correct partial pressure of lead oxide as discussed below.

mixtures of oxygen and nitrogen were used. The crucible was then heated in an atmosphere furnace which had the same gas composition. At first, the specimens in their crucible were set in the furnace and heated to the sintering temperature, but this resulted in a slow heating rate and consequently, considerable uncertainty about the effective time at temperature. Later, a technique was devised to insert and withdraw the crucible from the hot zone of the atmosphere furnace. Using this procedure, the specimens reached the sintering temperature in less than two min and cooled below 600°C in about 10 s. The subsequent rate of cooling was reduced to avoid fracture at the curie transformation around 350°C.

The density of the sintered specimens was measured by immersion in mercury or by calculating the specimen's volume from its dimensions and measuring its weight. The geometric technique was used for determining the initial density to avoid contamination with mercury and it was faster and more accurate than the immersion method. Mercury immersion was necessary for irregularly shaped pieces, e.g., broken, cracked or warped pellets.

Grain sizes were measured from scanning electron micrographs of surfaces that were polished and chemically etched, and original pellet surfaces that were thermally etched during sintering. The line intercept method[9] was used. Reported grain sizes are 1.5 times the average chord length. More than 200 grains were counted for each determination.

High field ferroelectric measurements were made to determine the ease and extent of domain reorientation. Specimens were prepared by lapping the pellet faces flat and parallel and painting on silver

electrodes.* An alternating electric field (approximately ± 100 volts/mil or 40 KV/cm) was applied and the resulting dielectric polarization was recorded. Hysteresis loops were run at 60 and 0.01 hz. The magnitude of the maximum polarization is proportional to the extent of domain boundary motion which is sensitive to the concentration of lattice vacancies.[10,11]

III. Results and Discussions

(1) Stoichiometry and Lattice Vacancies

Lead zirconate titanate has two components that are quite volatile at the sintering temperature, lead and oxygen. The equilibrium vapor pressures of zirconium, titanium and their oxides are low at 1200°C, so these components are not readily lost by evaporation. In order to establish and maintain the desired stoichiometry, lead zirconate and lead titanate must be heat treated in an atmosphere which contains the correct oxygen and lead oxide partial pressures. Equilibrium of the vapor-phase reaction

$$PbO_{vapor} \rightleftarrows Pb_{vapor} + 1/2\ O_{2\ vapor} \qquad (1)$$

is assumed so any two vapor pressures fix the lead and the oxygen activity.

The phase diagrams for lead oxide-titanium oxide[12] and lead oxide-zirconium oxide[12] are shown in Fig. 1. Both were determined in air. The corresponding lead oxide activity composition diagrams are also shown. These were constructed for 1200°C using the following assumptions:

---

* Silver Conducting Paint, Micro-Circuits Co.

(a) The lead oxide activity coefficient is equal to unity in the liquid phases. This is Raoult's Law for the lead oxide rich compositions; the activity of pure lead oxide is taken as unity.

(b) The lead oxide activity decreases linearly with composition in the solid solution regions (Henry's Law).

(c) The decomposition vapor pressures of lead titanate and lead zirconate as measured by Knudsen cell experiments,[13] were converted to activities by dividing by the vapor pressure above pure lead oxide at the same temperature.

At 1200°C lead zirconate and lead titanate are completely miscible.[12,14] Their solid solutions exist over a considerable range of PbO: $(Zr,Ti)O_2$ ratios, each corresponding to a different lead oxide activity. The metal:oxygen ratio may also vary. The latter variances are believed to be primarily accommodated by lattice vacancies. High concentrations of interstitials is unlikely, because the possible interstitial sites in the perovskite unit cell (Fig. 2) are bounded by both positive and negative ions. The crystal structure may be thought of as a cubic close packed, ordered arrangement of lead and oxygen. The octahedral site at the center of the cell is bounded by six oxygens and occupied by either zirconium or titanium. The other three octahedra are formed each by four anions and two lead ions; they are unoccupied. The tetrahedral sites are bounded by one lead and three oxygens. These are also empty. Alternatively, the structure may be compared to that of rhenium oxide (ReO_3).[15] Then the structural units are $(Zr,Ti)O_6^{=}$ octahedra. They are bound together at corners as each oxygen is coordinated with two tetravalent ions. Divalent lead enters the 12 fold sites between octahedra to maintain

electroneutrality. This description implies that crystal may become substantially deficient in lead if another charge balancing mechanism is operative. Such mechanisms might be the localization of electron holes at the vacancy,* the formation of an anion vacancy at an adjacent lattice, site, or the substitution of an ion with the incorrect valence on an adjacent site.

Clearly the concentration of lattice vacancies changes with the activity of lead oxide. With the oxygen pressure fixed, the crystal will saturate with A-site vacancies when the lead oxide activity is sufficiently low. Subsequent loss of lead oxide will result in the formation of a second phase, but the lead oxide activity of the system will remain constant. These lower limit activities were calculated from reported[13] vapor pressure measurements of mixtures of $Pb(Zr,Ti)O_3$ and $(Zr,Ti)O_2$. They are plotted in Fig. 3. The decomposition pressure (presumed to be lead oxide pressure) is greater for $PbZrO_3$ than for $Pb(Zr_{.5}Ti_{.5})O_3$. Thus when a specimen of $Pb(Zr_{.5}Ti_{.5})O_3$ is buried in a mixture of lead zirconate plus zirconia and heat treated at a high temperature, vapor transport of lead oxide will allow the specimen to "equilibrate" with the packing powder. Transport of titania and zirconia is negligible at 1200°C so the zirconium-titanium ratio of the specimen will not change. The specimen will simply lose lead oxide until its activity is approximately 0.05. Some of the zirconia in packing powder will react with the

---

*This type of A site vacancy is not charged with respect to the undisturbed lattice and will be designated as V_A. Uncharged B site and oxygen vacancies will be represented by V_B and V_O, respectively. The concentration of the defect will be indicated by square brackets [ ].

expelled lead oxide to form more lead zirconate and the lead oxide activity of the system will remain at 0.05. Loss of lead oxide from the system (say by evaporation to the surrounding) will cause some of the lead zirconate to decompose, but the lead oxide activity does not decrease.

This "buffered" situation is also possible for high lead oxide activities. The lead oxide activity of mixtures of $Pb(Zr,Ti)O_3$ and lead oxide rich liquid were calculated from the $PbO:ZrO_2:TiO_2$ ternary phase diagram.[14] Again Raoult's Law was assumed for the liquid and pure lead oxide (liquid) was taken as the standard state. Those activities are also plotted in Fig. 3. Now consider a specimen packed in a mixture of lead titanate and lead oxide. After equilibration with respect to lead oxide, the activity of the system will remain at approximately 0.7 (at 1200°C ... see Fig. 3). Loss of lead oxide from the system will simply reduce the quantity of the lead oxide rich liquid in the packing powder. During equilibration, the specimen remains single phase, but its lead oxide activity is increased to approximately 0.7. This change is accomplished by increasing the lead concentration of the crystal, i.e., reducing the concentration of lead vacancies.

Equilibration experiments were conducted with both types of packing powder to establish the width of the single phase region. Specimens of $Pb(Zr_{.5}Ti_{.5})O_3$ slightly deficient in lead oxide were weighed, equilibrated with "buffered" packing powders with high and low lead oxide activities in one atmosphere of oxygen, and then reweighed. The results of these experiments at 1150°C is shown in Fig. 4. If the difference in specimen weight at lead oxide activities of 0.7 and 0.05 is assumed

entirely due to the difference in the concentration of lead vacancies, then the saturation concentration of these defects is calculated to 5.6×10^{20} per cubic centimeter. This concentration corresponds to approximately 4% of the lead atoms missing. Allowances for simultaneous changes in the concentrations of B site and oxygen vacancies were not included in this calculation. Significant changes in either of those concentrations would mean the actual saturation concentration is somewhat less than 5.6×10^{20} per cubic centimeter.

It is also possible to fix the lead oxide activity at intermediate values. The specimen is packed in single-phase lead zirconate titanate powder in a closed cell. A small amount of lead oxide is lost by the specimen and packing powder to establish the atmosphere inside the cell. This loss, of course, reduces the lead oxide activity. Hence the final stoichiometry of the specimen will be sensitive to the initial lead oxide concentration in the system, the volume of the cell, and any vapor losses from it. Equilibration experiments with this type of packing powder were also conducted and shown in Fig. 4. The lead oxide activity of stoichiometric lead zirconate-titanate packing powder was taken as 0.5.

The oxygen activity in the preceding discussion has been assumed constant, but this requirement may be relaxed. When the partial pressure of oxygen in the atmosphere is reduced, the specimen will lose that component in order to achieve the correct oxygen activity

$$O_{solid} \rightleftarrows 1/2(O_2)_{vapor} + V_o^{\cdot}. \qquad (2)$$

This same type reaction might have been considered for lead:

$$Pb_{solid} \rightleftarrows Pb_{vapor} + V_{Pb}. \qquad (3)$$

Both these reactions alter the stoichiometry.

Chemical interaction between the several types of vacancies in the solid should also be considered. Schottky equilibrium is probably a reasonable assumption. For an ABO_3 compound the Schottky relation is:[16]

$$[V_A]\,[V_B]\,[V_O]^3 = K_s \qquad (4)$$

Equations (2), (3), and (4) preduct that lowering the lead activity, at a fixed oxygen pressure, will increase $[V_A]$, decrease $[V_B]$, and leave $[V_O]$ unchanged. With the lead activity constant, lowering the oxygen partial pressure should increase $[V_O]$, decrease $[V_B]$ and not alter $[V_A]$.

Doping is another mechanism for introducing vacancies. When an ion with the incorrect valence enters the lattice, charged vacancies may form to maintain local electroneutrality. These phenomena have been established[17,18] when Nb^{+5} substitutes for Ti^{+4}; one lead vacancy (with an effective charge of minus two) is introduced for every two niobium ions. Aluminum ions also enter B lattice sites[3] and are assumed to create charged anion vacancies. In each case the effective charge of the vacancies and the substituted ion is opposite so coulombic attraction between them is expected.

(2) Grain Growth

The effect of aluminum and niobium on sintering and grain growth is shown in Fig. 5. These data were obtained by slowly heating the doped pellets and held for the indicated time at 1200°C. The rate of grain

growth is reduced when either aluminum or niobium is present. Similar grain growth inhibition has been reported for lead zirconate titanate doped with Fe^{+3} (B site),[19] Ta^{+5} (B site),[1] Bi^{+3} (A site)[5,20] and La^{+3} (A site).[1]

It is believed that the doping ions concentrate near the grain boundaries and substantially reduce their mobility. When the boundary moves, it must drag the excess (adsorbed) impurities along with it, as depicted in Fig. 6. This mechanism for reducing grain boundary mobility has been studied theoretically and experimentally as it applies to the recrystallization of metals.[21-23] Jorgensen[24,25] and Westbrook[25] used this model to explain how magnesia inhibits grain growth in alumina and allows sintering to theoretical density. Jorgensen and Anderson[26] later showed that Th^{+4}, dissolved in yttria, was adsorbed at grain boundaries and substantially reduced the rate of grain growth, thereby permitting complete densification. When the thoria content exceeded the solid solubility limit, the grain growth rate was further decreased and second phase particles were observed at grain boundaries.

Doping with aluminum and niobium did not effectively impede grain growth. This seems to imply that the doping ions are associated with the charged vacancies they create, and these vacancies are responsible for the attraction between the defects and grain boundaries. Al^{+3} and Nb^{+5} are believed to associate with each other (in pairs) without charged oxygen or lead vacancies. The defects are not strongly attracted to the boundaries and cannot reduce their mobility.

The grain growth kinetics for undoped material was determined from pellets that were rapidly heated and cooled, Fig. 7. The average grain

size increases proportional to the cube root of time. The growth rate is not sensitive to the lead or oxygen activity.

(3) Sintering

The sintering kinetics of the undoped material follow the Coble model.[27] This model describes the intermediate and final stages of sintering single-phase crystalline solids by the bulk diffusion of vacancies from pores to grain boundaries. The density increased linearly with the logarithm of time, Fig. 8. When the specimens were heated slowly, considerable sintering occurred during heating and the density; logarithm time plot was not linear, Fig. 5. Instantaneous densification rates were calculated from the slope of the density plots in Fig. 5. These rates, calculated at various times, are plotted in Fig. 9 as a function of the measured grain size cubed. The slope of negative one indicates that the densification rate is inversely proportional to the grain size cubed, as predicted by the Coble model.

Figure 5 indicates that doping with aluminum or with niobium keeps the grain size small and thereby expedites densification. Niobium is a more effective grain growth inhibitor than aluminum so it is more effective at accelerating sintering. Doping with aluminum and niobium did not retard grain growth as much as either alone, and densification was slow.

Increasing the lead activity with the pressure of oxygen held at one atmosphere did not alter the densification behavior. A change in stoichiometry (increase in $[V_B]$, decrease in $[V_A]$, $[V_O]$ constant) was verified by measured weight grains. Specimens in different atmospheres gained weight at different rates during the first 200 min of sintering

and then remained at constant but different stoichiometries during the subsequent sintering (Fig. 4). The densification was unaffected by these variations in stoichiometry (Fig. 8). This clearly indicates that the densification rate is independent of the concentration of A-site and B-site vacancies. Reducing the partial pressure of oxygen in the sintering atmosphere (i.e., increasing $[V_O]$) accelerated sintering (Fig. 8). These observations seem to indicate that oxygen vacancies are the slowest moving species, and hence, rate limiting. Increasing their concentration increases the diffusion flux and increases the densification rate.

One might expect that doping with aluminum (forming additional oxygen vacancies) would increase the rate of diffusion and densification, but this is not the case. In Fig. 9 the densification rates of the several materials can be compared at the same grain size. When the average grain size is 12 μm the densification rate is far greater for the undoped material. This may be explained as follows. First, the vacancies introduced by doping are "bound" to the impurity ions and cannot freely move through the crystal to expedite mass transport. Introducing these "bound" vacancies should, through the Schottky relation, Eq. (4), reduce the concentration of "unbound" vacancies and retard diffusion. Second, the defect concentration gradients at grain boundaries (FIg. 6) should oppose the diffusion of vacancies from pores to grain boundaries. The adsorbed defect might repel vacancies sufficiently for grain boundary diffusion to become the dominant densification mechanism. This could explain the non-linear densification rate:grain size relation observed in Fig. 9 with aluminum doped and niobium doped materials.

(3) Ferroelectric Properties

The ferroelectric hysteresis loops (Fig. 10) confirm the compensatory nature of aluminum and niobium ions. Doping with niobium increases the ease and extent of ferroelectric domain boundary motion while aluminum has the opposite effect. When both ions are present, the hysteresis loop resembles that of the undoped material. The uncharged lattice vacancies, introduced by heating in reduced oxygen or lead oxide pressures, did not affect the hysteresis loops as dramatically as the charged ones introduced by doping.

IV. Summary and Conclusions

Single-phase lead zirconate titanate exists over a wide range of stoichiometry, corresponding to varying concentrations of lattice vacancies. The material can accommodate relatively high concentrations of substitutional impurities which have the incorrect valence; local electroneutrality is maintained by charged lattice vacancies.

Trivalent aluminum and pentavalent niobium substitute for tetravalent titanium and doping with either ion retards grain growth. It is believed that the charged vacancies associated with these impurities cause them to be adsorbed at grain boundaries. Then the moving boundary must drag along the excess concentration of impurities and this reduces its mobility. Aluminum and niobium compensate for one another; doping with both does not effectively retard grain growth. Then the impurities are associated with each other (Nb^{+5}-Al^{+3} pairs) and not with charged vacancies. The defects are not strongly adsorbed so the boundary mobility approaches that of the undoped material.

Doping with aluminum or with niobium enhances sintering by keeping the grain size small, thereby allowing densification to continue at a rapid rate. Sintering follows the Coble model; shrinkage occurs by bulk diffusion of lattice vacancies from pores to grain boundaries. Oxygen vacancies are believed to be the slowest moving species. Doping reduces the effective diffusivity; the grain size effect is, however, dominant. The vacancies introduced by doping are believed to be bound to the impurity ions so they are not free to move through the lattice and contribute to mass transport.

Ferroelectric measurements confirm the compensation effect noted for specimens doped with both aluminum and niobium.

Acknowledgments

Helpful discussions with Dr. Paul Jorgensen are gratefully acknowledged. Thanks for experimental assistance are due Rand Unverferth, Mike Neminic, John Lawson, George Scherer, Robert Holman and John Sherohman.

The authors wish to express appreciation for the use of the scanning electron microscope within the Electronics Research Laboratory, University of California, provided under Grant No. GB-6428 from the National Science Foundation and under Grant No. GM-15536 from the National Institute of Health.

This work was done under the auspices of the United States Atomic Energy Commission.

References

1. F. Kulcsar, "Electromechanical Properties of Lead Titanate Zirconate Ceramics Modified with Certain Three or Five-Valent Additions," J. Am. Ceram. Soc., 42 [7] 343-49 (1959).

2. E. C. Subbarao, "Studies on Lead Titanate Ceramics Containing Niobium or Tantalum," J. Am. Ceram. Soc., 43 [3] 119-22 (1960).

3. R. B. Atkin and R. M. Fulrath, "Solubility of Aluminum in Lead Zirconate Titanate," J. Am. Ceram. Soc., 53 [1] 51-2 (1970).

4. G. A. Pryor, "Impurity Effects in Sintering Lead Zirconate Titanate," M.S. Thesis, Univ. of Calif., Berkeley, 1968 (UCRL-18191).

5. R. B. Atkin and R. M. Fulrath, "The Practical Aspects of Sintering," in Interfaces Butterworth Publishing Co., Melbourne, Australia (1969). Also see UCRL-18795.

6. K. E. Nelson and R. L. Cook, "Effect of Contamination Introduced During Wet Milling on the Electrical Properties of Barium Titanate," A. Ceram. Soc. Bull. 38 [10] 499-500 (1959).

7. T. F. Murray and R. H. Dungan, private communication.

8. R. L. Coble, "Sintering Alumina: Effect of Atmosphere," J. Am. Ceram. Soc., 45 [3] 123-7 (1962).

9. R. L. Fullman, "Measurement of Particle Sizes in Opaque Bodies," Trans. AIME, 197 [3] 447-52 (1953).

10. H. Jaffe, "Properties of Ferroelectric Ceramics in the Lead-Titanate Zirconate System," Presented at the International Conference on Components and Materials used in Electronic Engineering, The Institution of Electrical Engineers Paper No. 3625, June 1961.

11. R. Gerson, "Variation in Ferroelectric Characteristics of Lead Zirconate Titanate Ceramics Due to Minor Chemical Modifications," J. Appl. Phys. 31 [1] 188-94 (1960).

12. R. Moon, "High Temperature Phase Equilibria in the Lead Titanate-Lead Zirconate System," Ph.D. Thesis, Univ. of Calif. Berkeley, 1967 (UCRL 17545).

13. K. H. Härdtl and H. Rau, "PbO Vapour Pressure in the $Pb(Ti_{1-x}Zr_x)O_3$ System," Solid State Communications, 7 41-5 (1969).

14. S. Fushimi and T. Ikeda, "Phase Equilibrium in the System PbO-TiO_2-ZrO_2," J. Am. Ceram. Soc., 50 [3] 129-32 (1967).

15. A. F. Wells, Structural Inorganic Chemistry, Oxford University Press, London (1962).

16. R. B. Atkin, "Sintering and Ferroelectric Properties of Lead Zirconate Titanate Ceramics," D. Eng. Thesis, Univ. of Calif., Berkeley, 1970 (UCRL-20309).

17. T. Ikeda, Y. Tanaka, T. Ayakawa and H. Noake, "Precipitation of Zirconia Phase in Niobium-Modified Ceramics of Lead Zirconate-Titanate," Japan J. Appl. Phys., 3 [10] 581-87 (1964).

18. R. B. Atkin, R. L. Holman and R. M. Fulrath, "Ionic Substitutions in Lead Zirconate-Titanate," submitted to J. Am. Ceram. Soc. Aug 1970 (UCRL-19632).

19. T. B. Weston, A. H. Webster and V. M. McNamara, "Lead Zirconate-Lead Titanate Piezoelectric Ceramcis with Iron Oxide Additions," J. Am. Ceram. Soc., 52 [5] 253-57 (1969).

20. G. H. Haertling, "Hot-Pressed Lead Zirconate-Lead Titanate Ceramics Containing Bismuth," J. Am. Ceram. Soc., 43 [12] 875-9 (1964).

21. P. Gordon and R. A. Vandermeer, "The Mechanism of Boundary Migration in Recrystallization," Trans. Met. Soc. AIME, 224 917 (Oct 1962).

22. K. Lucke and K. Detert, "A Quantitative Theory of Grain Boundary Motion and Recrystallization in Metals in the Presence of Impurities," Acta. Met. 5 628-37 (Nov 1957).

23. E. S. Machlin, "Theory of Solute Atom Limited Grain Boundary Migration," Trans. Met. Soc. AIME 224 1153-67 (Dec 1962).

24. P. J. Jorgensen, "Modification of Sintering Kinetics by Solute Segregation in Al_2O_3," J. Am. Ceram. Soc., 48 [4] 207-10 (1965).

25. P. J. Jorgensen and J. H. Westbrook, "Role of Solute Segregation at Grain Boundaries During Final-Stage Sintering of Alumina," J. Am. Ceram. Soc., 47 [7] 332-28 (1964).

26. P. J. Jorgensen and R. C. Anderson, "Grain-Boundary Segregation and Final-Stage Sintering of Y_2O_3," J. Am. Ceram. Soc. 50 [11] 553-8 (1967).

27. R. L. Coble, "Sintering Crystalline Solids. I. Intermediate and Final STage Diffusion Models," J. Appl. Phys. 32 [5] 787-92 (1961).

FIGURE CAPTIONS

Fig. 1. The approximate binary phase diagrams indicate that the perovskite compounds may exist over a range of composition. The activity:composition diagrams show the limiting lead oxide activities for the single phase regions.

Fig. 2. The perovskite unit cell with possible interstitial sites indicated.

Fig. 3. Limiting lead oxide activities for single phase $Pb(Zr,Ti)O_3$.

Fig. 4. Vapor-phase equilibration experiments.

Fig. 5. Effects of impurities on sintering and grain growth.

Fig. 6. Mechanism by which adsorbed impurities impede grain boundary motion.

Fig. 7. Grain growth of undoped material.

Fig. 8. The effect of atmosphere on the sintering of undoped material.

Fig. 9. Densification rate, calculated from the slope of the sintering curves in Fig. 5, versus the instantaneous grain size. The Coble sintering model[27] predicts a slope of minus one. The intercept should be proportional to the diffusivity.

Fig. 10. Doping with niobium or aluminum alters the ferroelectric hysteresis loop: the effects are mutually cancelling. Dielectric polarization is plotted as a function of electric field.

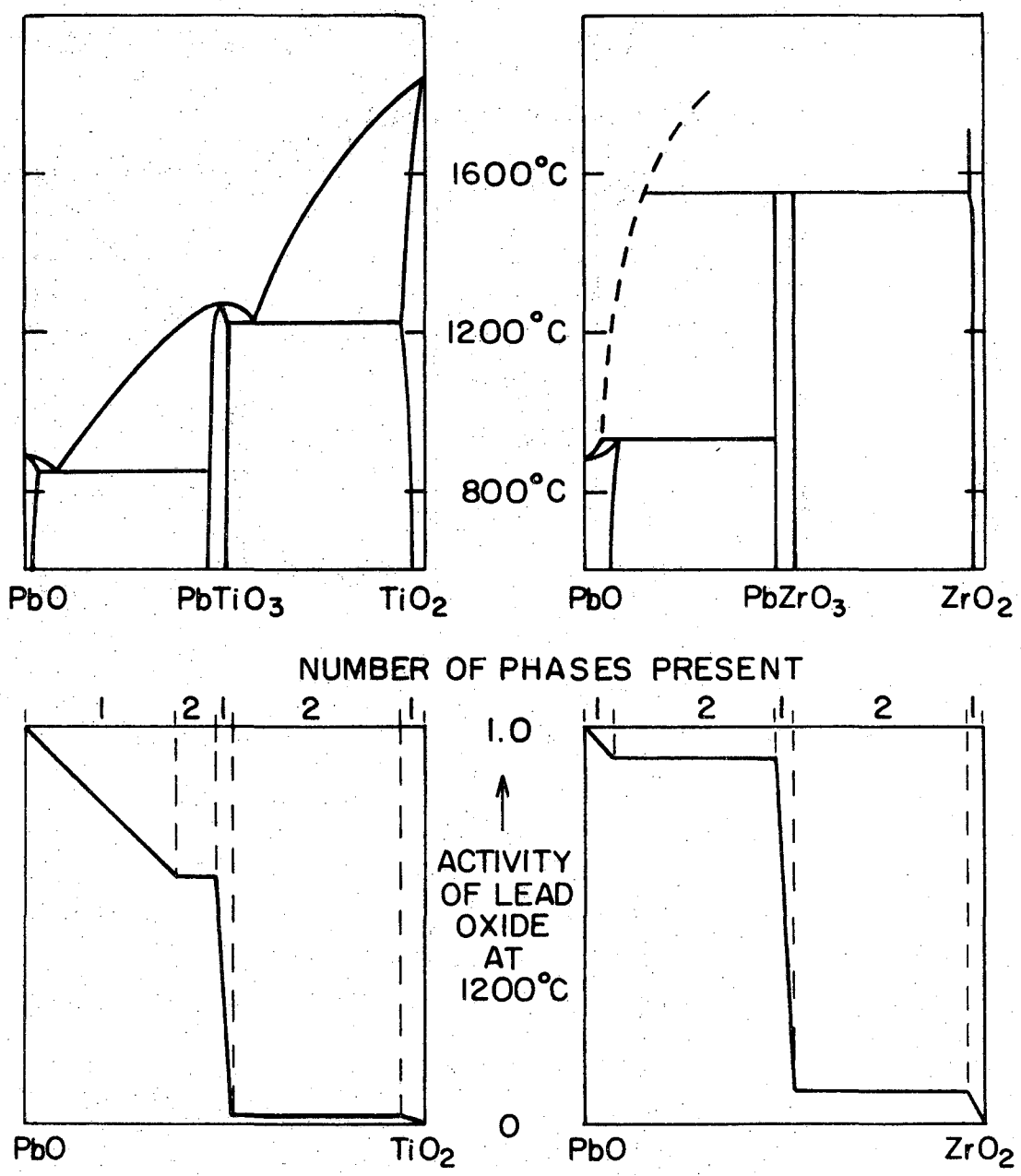

XBL 708-6450

Fig. 1

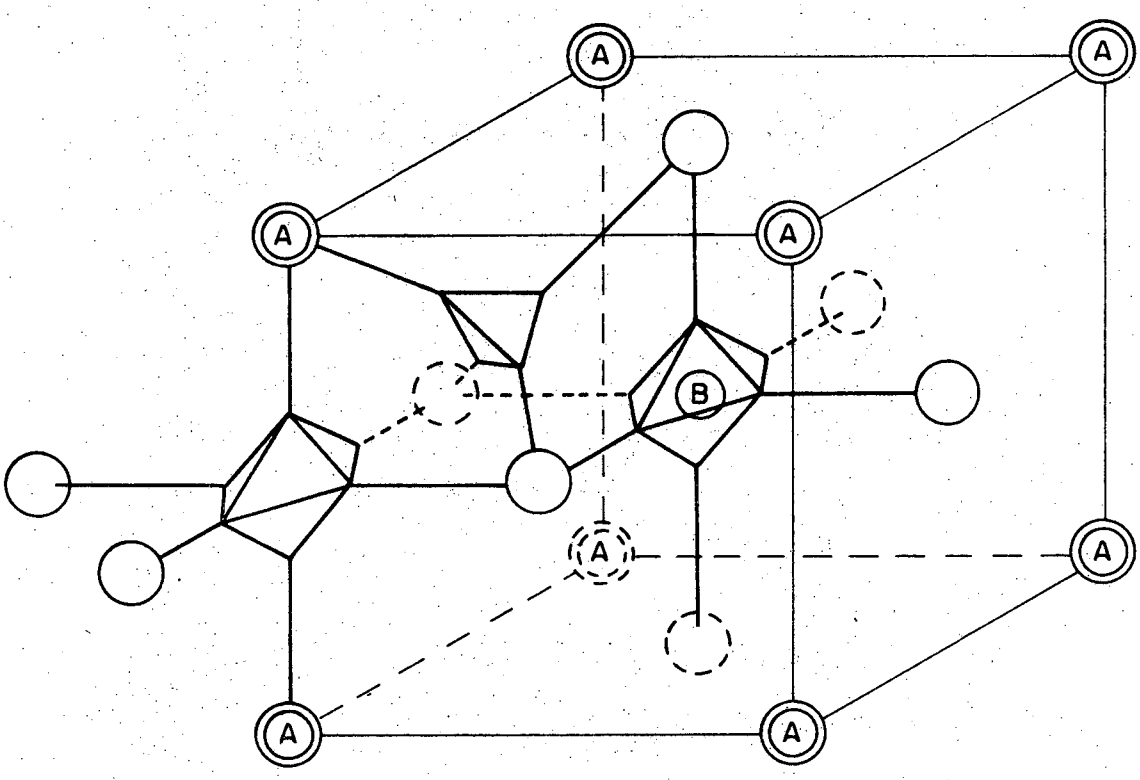

XBL 708-6448

Fig. 2

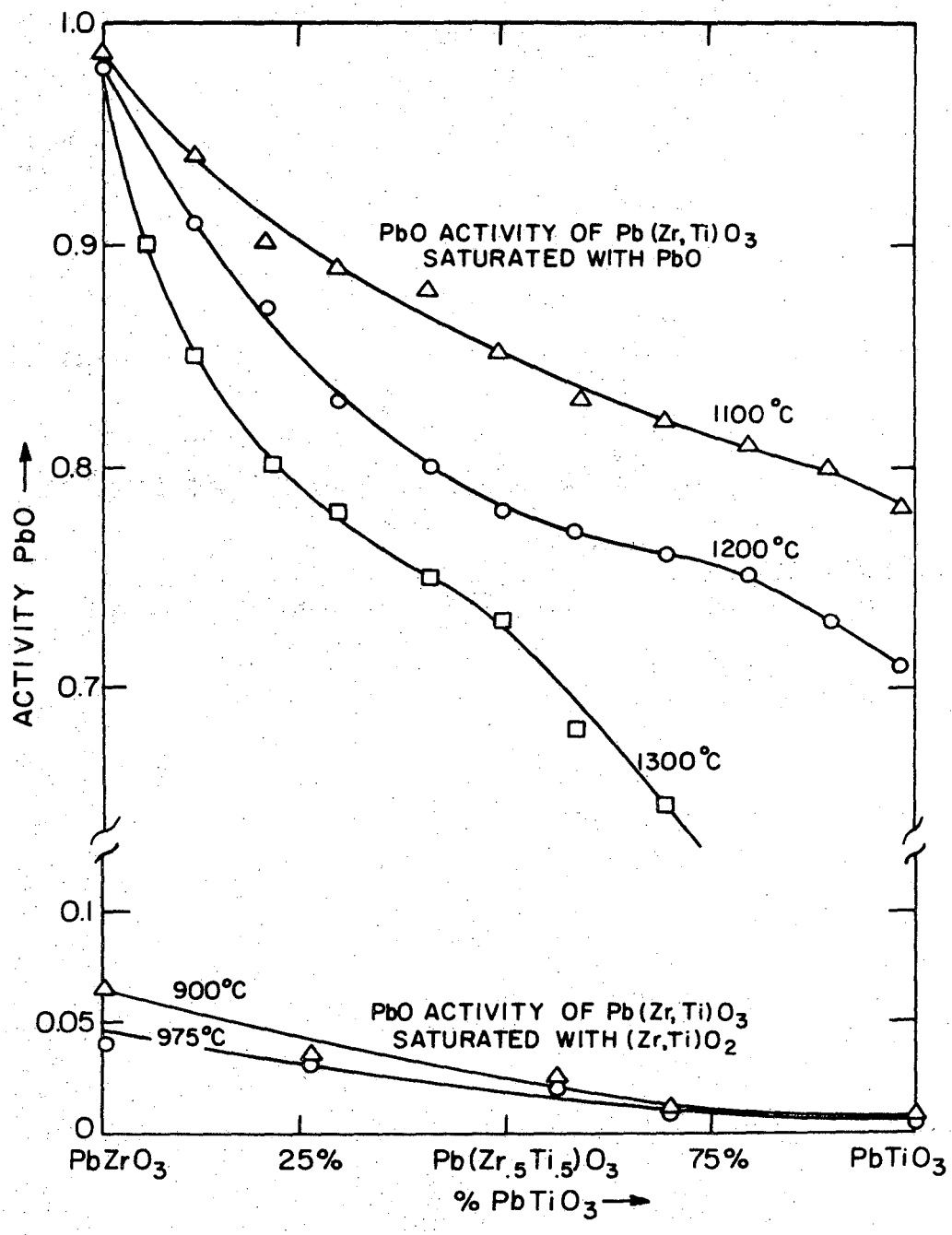

XBL 708-6454

Fig. 3

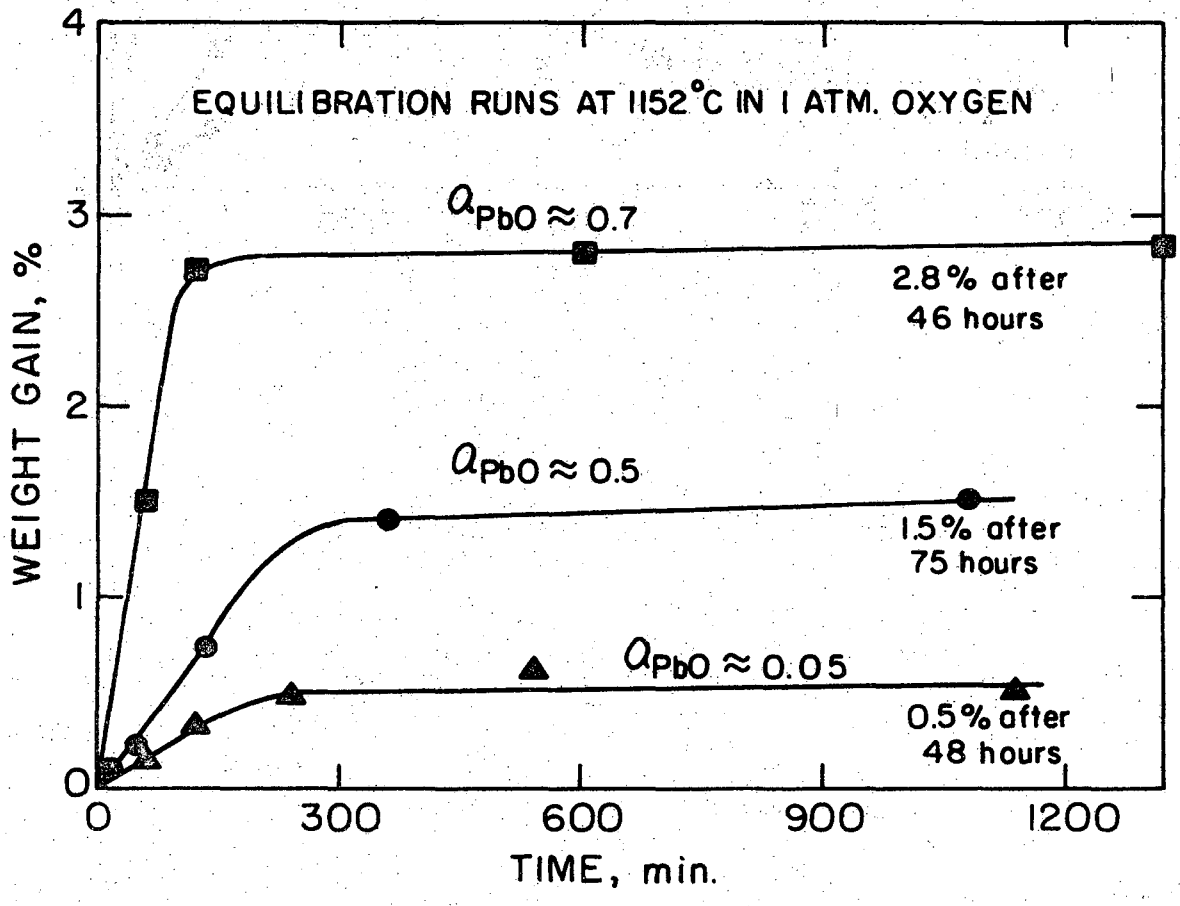

XBL 708-6453

Fig. 4

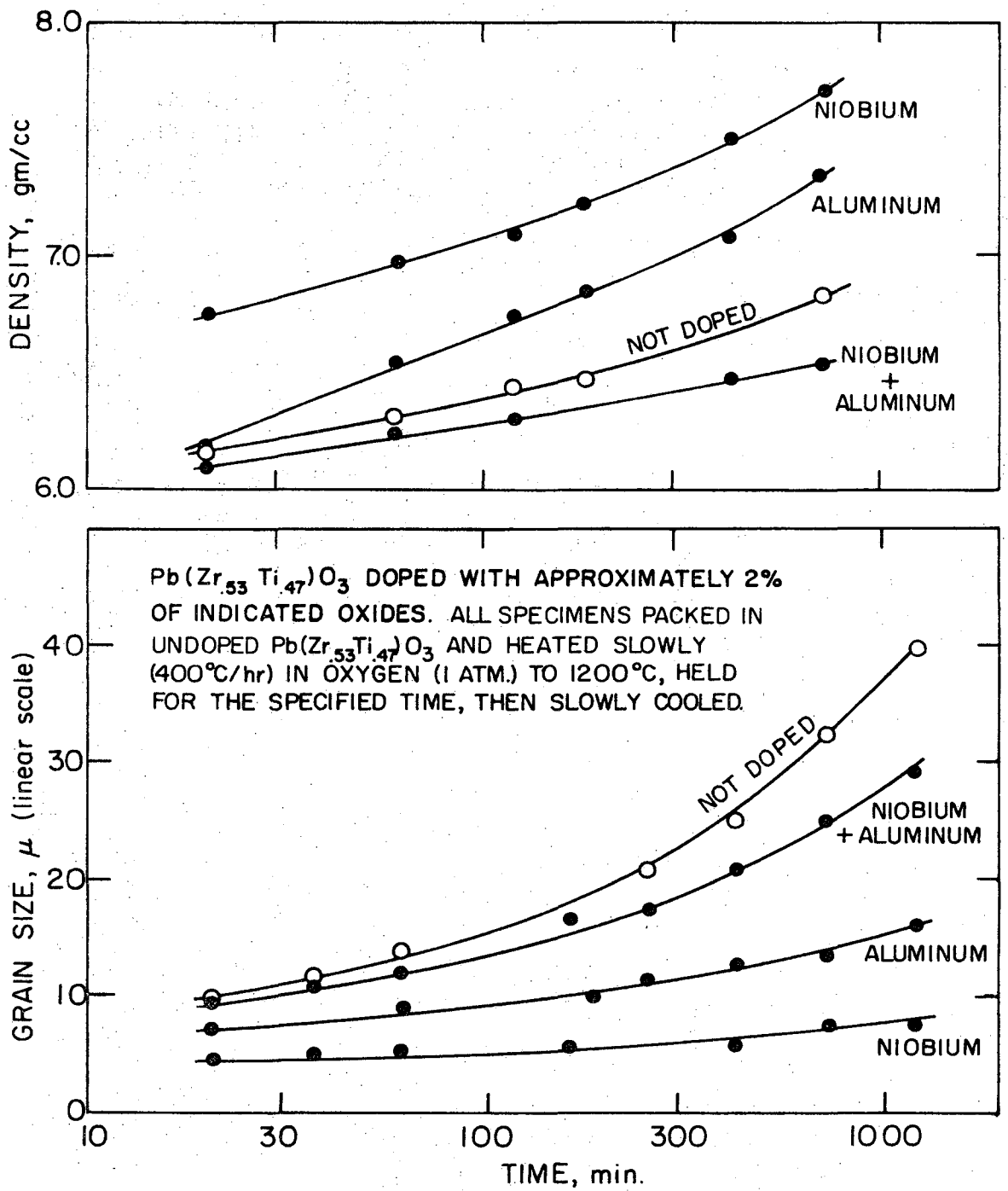

XBL 709-6588

Fig. 5

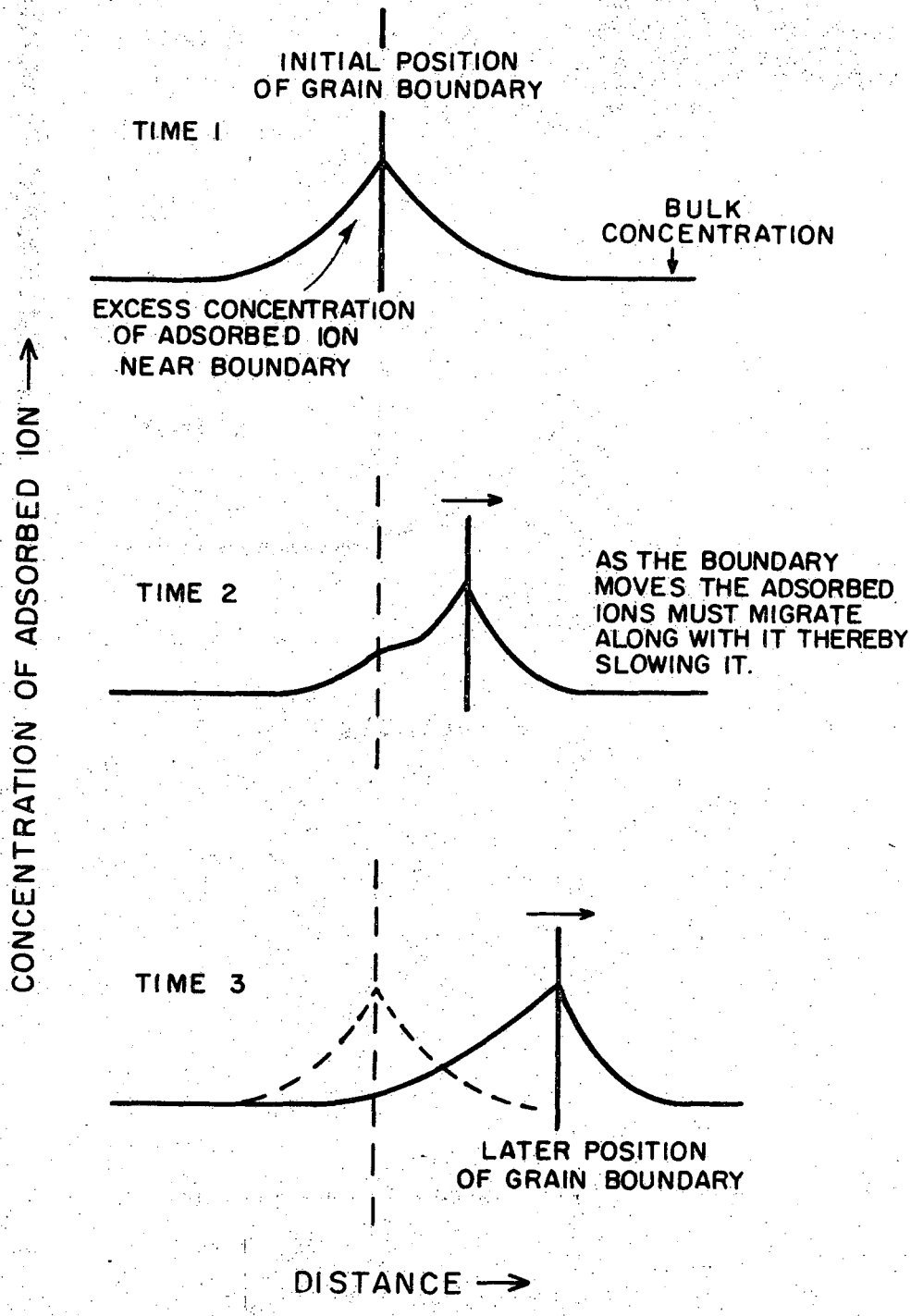

XBL 708-6451

Fig. 6

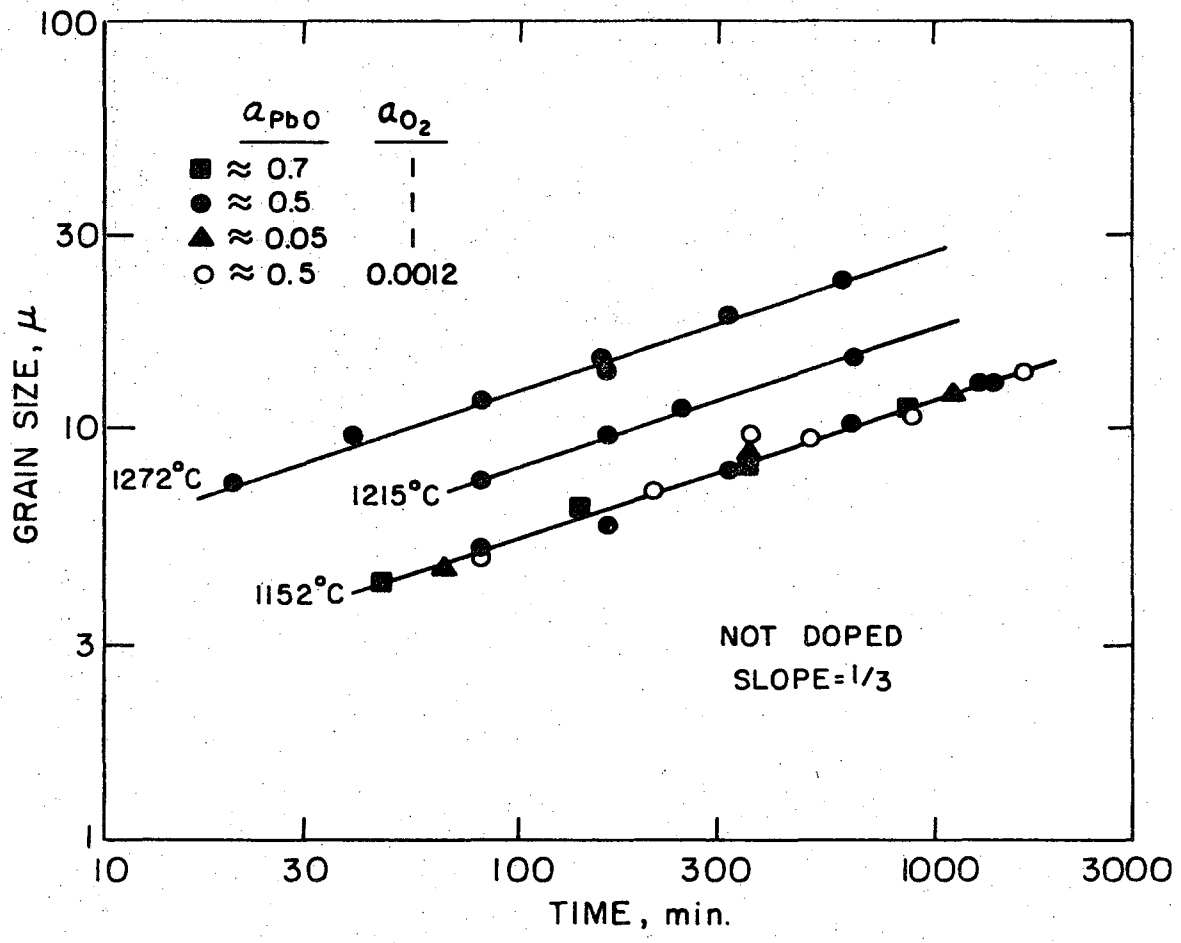

XBL 709-6587

Fig. 7

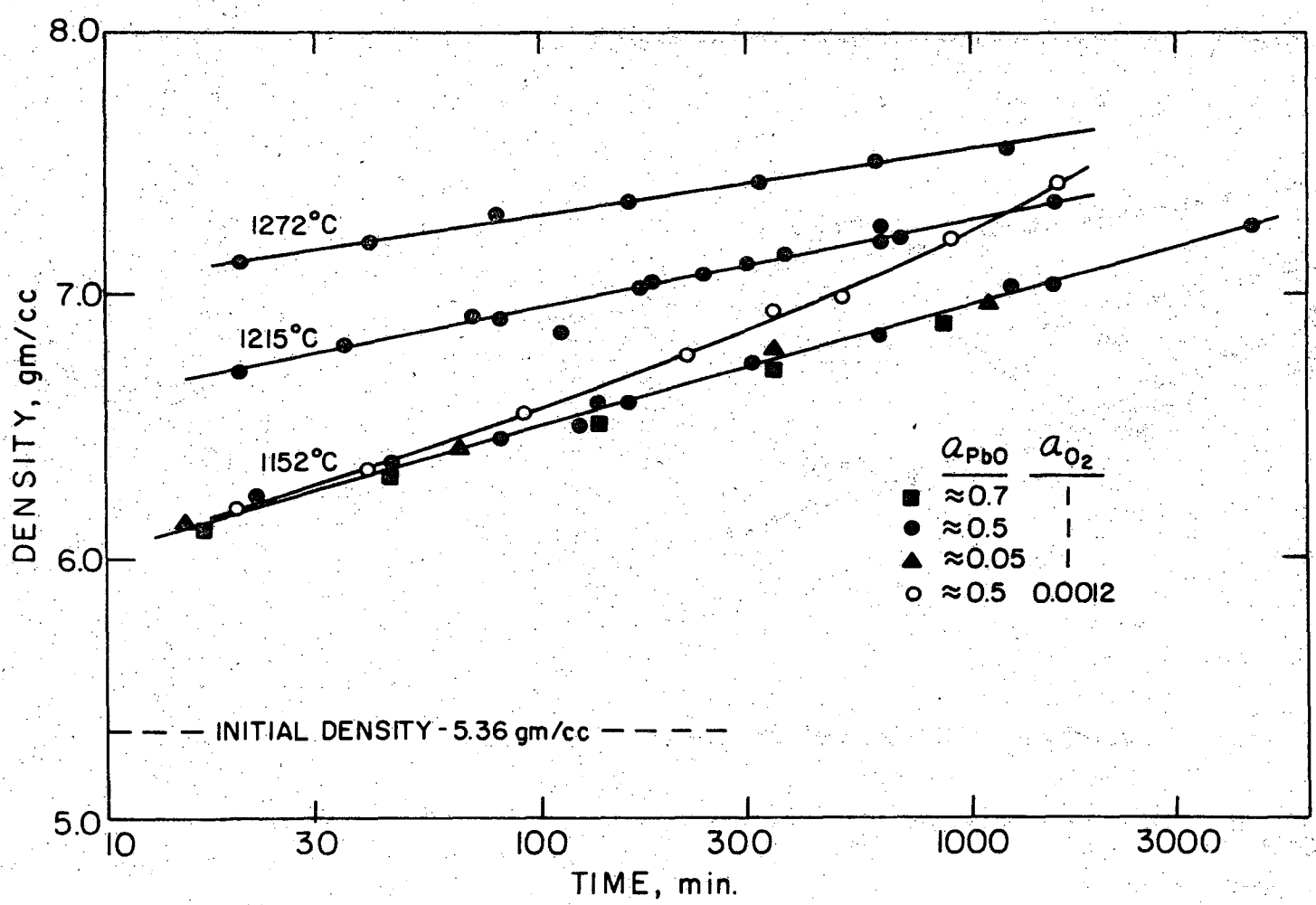

XBL 708-6447

Fig. 8

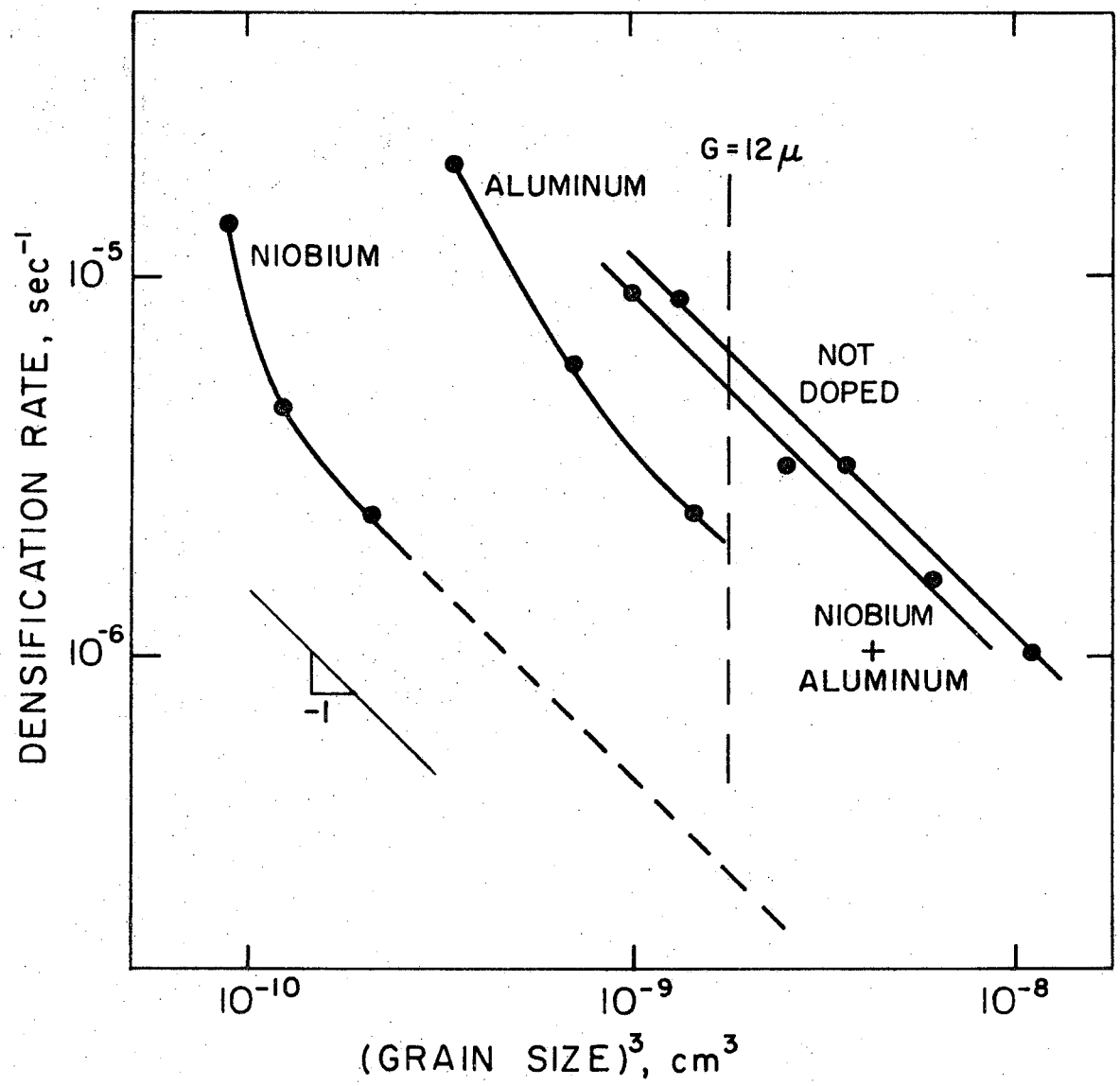

XBL 709-6586

Fig. 9

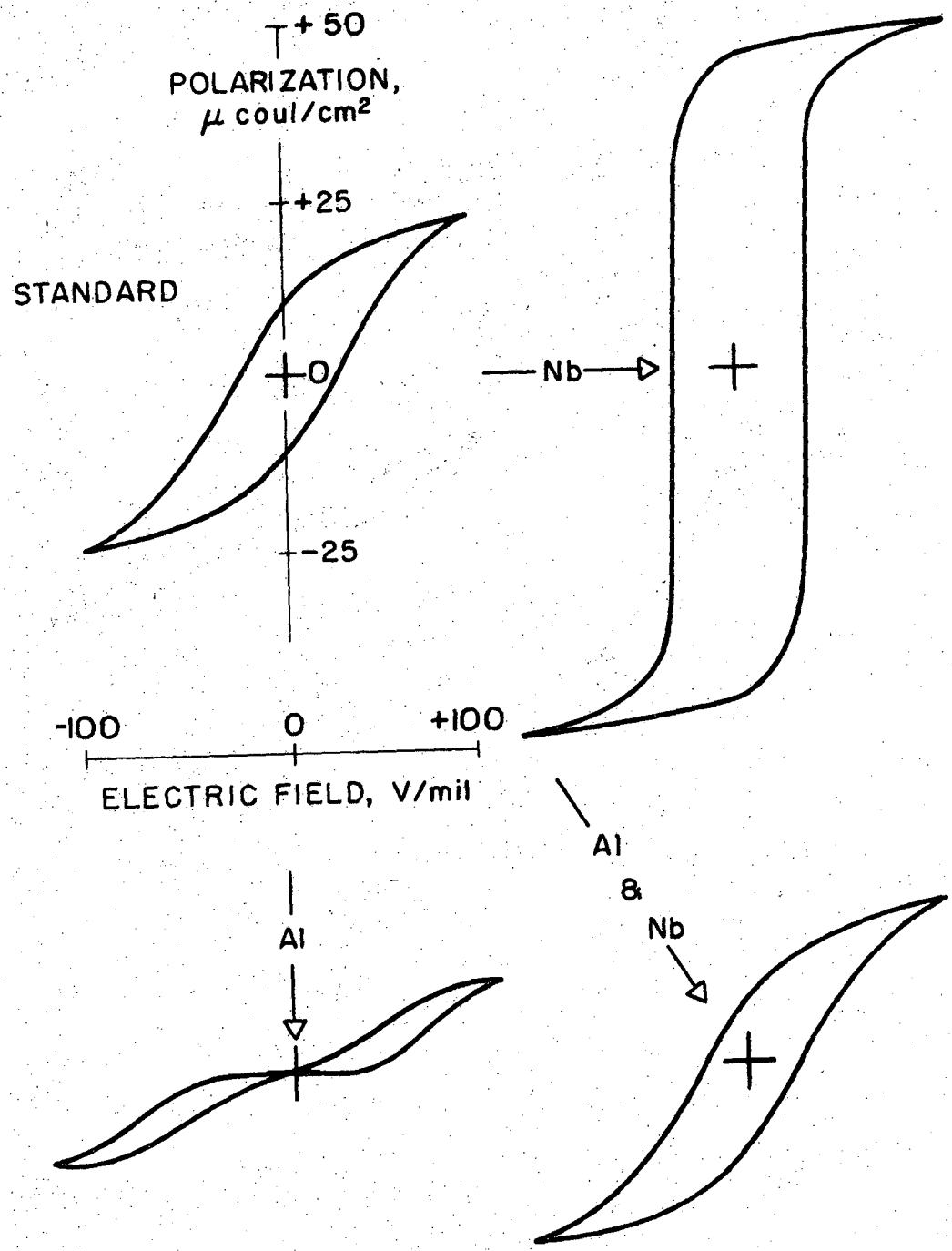

XBL 708-6443

Fig. 10